Thermophysics and Aeromechanics, *2017*, *Vol. 24*, *No. 6*

DOI: 10.1134/S086986431706004X

Numerical study of the influence of flow blockage on the aerodynamic coefficients of models in low-speed wind tunnels

V.T. Bui*, V.T. Kalugin, V.I. Lapygin, and A.I. Khlupnov

Bauman Moscow State Technical University, *Moscow*, *Russia*

E-mail: vantien06@gmail.com*, vil1940@mail.ru, kaluginvt@mail.ru

(*Received July 18*, *2016*; *in revised form March 30*, *2017*)

With the use of ANSYS Fluent software and ANSYS ICEM CFD calculation grid generator, the flows past a wing airfoil, an infinite cylinder, and 3D blunted bodies located in the open and closed test sections of low-speed wind tunnels were calculated. The mathematical model of the flows included the Reynolds equations and the SST model of turbulence. It was found that the ratios between the aerodynamic coefficients in the test section and in the free (unbounded) stream could be fairly well approximated with a piecewise-linear function of the blockage factor, whose value weakly depended on the angle of attack. The calculated data and data gained in the analysis of previously reported experimental studies proved to be in a good agreement. The impact of the extension of the closed test section on the airfoil lift force is analyzed.

Key words: wind tunnel, blockage factor, aerodynamic coefficients.

Introduction

The unbounded (free) subsonic flow past an aircraft model and the flow past the same model in the bounded wind-tunnel (WT) test section are different flows; the degree of this difference is normally characterized by the ratio between the characteristic size of the model (S) and that of the WT test section (F): $\xi = S/F$. Traditionally, as the WT test-section size F, the cross-sectional area of the WT test section at the nozzle exit is adopted. Apparently, with a decrease of ξ the difference between the values of flow quantities in the vicinity of the model in the free stream and in the WT test section diminishes. An experience gained in experimental studies has shown that there exists a value of ξ^* such that, with it, the influence due to the WT test-section boundaries, the nozzle boundaries, the diffuser boundaries, etc. on the values of aerodynamic coefficients at $\xi < \xi^*$ can be neglected. Available recommendations concerning the choice of ξ^* differ from each other because of the difference between the shapes of the models and experimental equipment: $\xi^* = 0.02 - 0.03$ [1], $\xi^* = 0.05 - 0.06$ [2, page 36], $\xi^* = 0.075$ [3, page 371]. The analysis of approximate dependences of aerodynamic coefficients on the parameter ξ [4, 5], the experimental data of [1, 4, 6–8], and the modeling data for the flow past blunt models in the closed test section of low-speed wind tunnels [9] all point to a linear behavior of dependences $C_{xa}(\xi)$, $C_{ya}(\xi)$, $m_z(\xi)$, where C_{xa} is the drag coefficient, C_{ya} is the lift coefficient,

and m_z is the pitching moment coefficient. Thus, both the experimental data and the theoretical estimates show that the dependences $C_{xa}(\xi)$, $C_{ya}(\xi)$, and $m_z(\xi)$ can be fitted with a piecewise-linear function whose value is constant value over the segment $[0, \xi^*]$. Consider the validity of this assumption by modeling the flow past models in an open (T-500) [10] and a closed (T-324) [11] WT test sections with the use of CFD methods.

The choice of the wind tunnels was motivated by the availability of data on their design features and measured data concerning the flow velocity field in the test section.

Problem statement

The mathematical model of the 3D WT flow and the free-stream flow is based on the Reynolds equations and on the SST model of turbulence, whose choice for the flows past a model in a wind tunnel was substantiated in publications [12–14]. The model was located at the center of the WT test section, whose centerline was coincident with the axis of symmetry of the model. Since the disturbance produced by the model propagated in both upstream and downstream direction, along with the flow in the WT test section, the flow in the nozzle and the flow in the diffuser were calculated.

In the present study, we use a right-handed Cartesian coordinate system whose axis O*x* coincides with the centerline of the WT test section and is directed upstream, and the axis O*y* is directed upward. The origin coincides with the center of the model, which is located at the centerline of the WT test section and at its middle. The mutual arrangement of the nozzle, the test section, and the diffuser and, also, the dimensions of those WT components for T-500 are shown in Fig. 1, where l = 500 mm is the height of the square nozzle-exit section. The contours of the top and bottom panels of the nozzle correspond to the Vitoshinsky airfoil [15]. The lateral panels of the nozzle are flat panels. The height of the square cross section of the entrance to the diffuser was 600 mm, and its vertex angle, 4°.

The contour of the meridional section of the T-324 wind tunnel and the mutual arrangement of the settling chamber, the nozzle, the test section, and the diffuser and, also, the dimensions of those WT components are shown in Fig. 2, where l = 1 m. The cross sections of

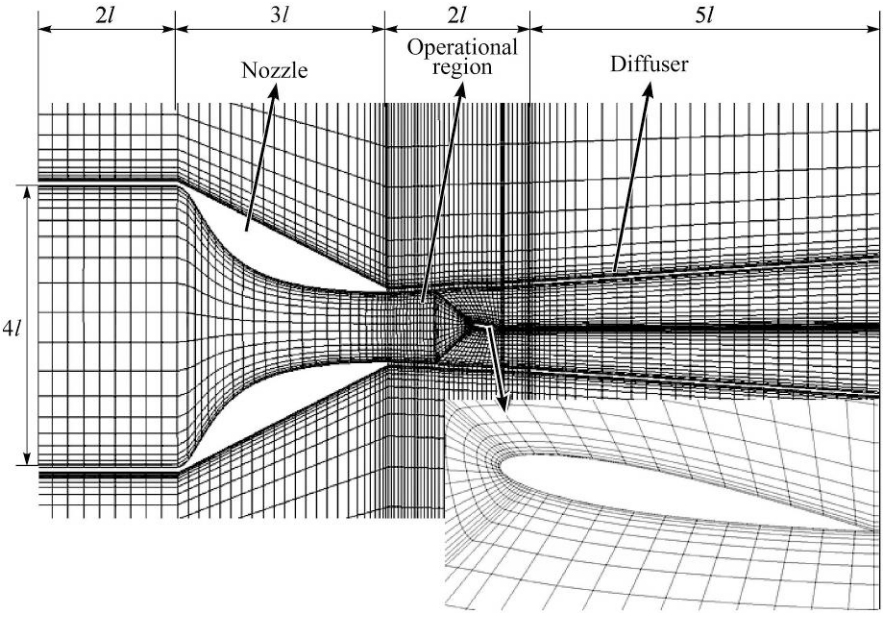

Fig. 1. Schematic of the T-500 wind-tunnel facility. Calculation domain and calculation grids.

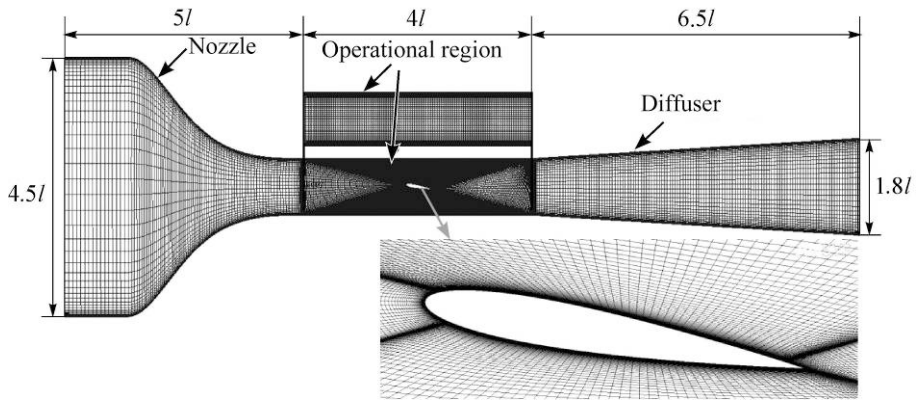

Fig. 2. The mutual arrangement of the nozzle, the test section, the diffuser, and the calculation grid.

the settling chamber, the nozzle, and the diffuser are all shaped as octagons, whereas the test section is shaped as a square with cut angles.

In calculating the flow past a model installed in the WT test section, the following boundary conditions were specified at calculation-domain boundaries (Figs. 1and 2):

– at the inlet to the settling chamber — a uniform profile of flow velocity, whose value was determined via an iterative calculation process implemented in the empty test section for reaching a steady-state flow velocity at the nozzle exit;

– at the right boundary of the calculation domain, at the exit from the diffuser — condition of constant mass flow rate;

– on the surfaces of the nozzle, diffuser and model — no-slip condition;

– at other calculation-domain boundaries in the case of the open test section, atmospheric pressure was specified.

The problem involves the calculations of the flows past models in the WT test section and in the free stream. These calculations were performed using ANSYS Fluent software. Structured calculation grids were generated using the ANSYS ICEM CFD module.

Calculation grids

The thickness of the first near-wall cell in the empty test section of T-500 was 1 mm. The sizes of each subsequent cell were increased by a factor of 1.2 in comparison with the previous cell. The total number of cells was 41204. The total number of cells in the empty test section of T-324 was 37000, and the height of the first near-wall cell, $3 \cdot 10^{-4}$ m. The performed calculation of the flow in the empty WT test section has demonstrated a satisfactory coincidence between the calculated and experimental velocity profiles [12, 13].

In calculating the flow around a model in the test section and in the free stream, a structured calculation grid was used. The size of the calculation cells was chosen such that the total number of cells across the boundary layer in the middle of the model was not lesser than ten. The height of the first near-wall cell was 10^{-6} m. The sizes of each subsequent cell were increased by a factor of 1.1 in comparison with the previous cell. The total number of the calculation cells in T-500 in the presence of the airfoil was 110000, and in the presence of a cylinder, 130000. The total number of the calculation cells in T-324 in the presence of a model was about 140000. Along with the number of cells, the quality of a calculation grid is characterized by the value of the non-dimensional coefficient for the height of the first near-wall cell Y^+:

$$Y^+ = \frac{\mathrm{Re}_x\,\Delta y}{x}\sqrt{\frac{C_\mathrm{f}}{2}},$$

where Δy is the height of the first near-wall cell and C_f is the friction coefficient. In the calculations, we had $Y^+ \le 2$, so that the values of Y^+ were in acceptable bounds for the SST model of turbulence [16].

In calculating the flow around the NASA0012 airfoil immersed in the free stream, the calculation domain was a combination of a rectangle with a hemi-sphere centered on the location of the airfoil model. The linear sizes of the calculation domain were 22.5b in longitudinal direction and 15b in transverse direction, where b is the airfoil-chord length. The total number of the calculation cells was 89000 [11].

In calculating the flow past a cylinder immersed in a free stream, the calculation domain was a circumference of radius $R = 60D$ with a cylinder of diameter D located at the center of the circumference. At the left hemi-sphere of the calculation domain, velocity values equal to the velocity at the nozzle exit were specified; at the right hemisphere, atmospheric pressure was assumed. The height of the first near-wall cell was 10^{-6} m. The sizes of subsequent cells were increased by a factor of 1.1 in comparison with the previous cell. On the basis of performed methodical calculations, the total number of cells, 79000, was determined.

In calculating the 3D flow past a model immersed in a free stream, the calculation domain was a circular cylinder in which the model was disposed. The diameter of the cylinder was 15D, and its length, 25D, where D is the maximum diameter of the model. At the left boundary, a velocity value equal to the velocity at the WT nozzle exit was specified. At other surfaces of the calculation domain, atmospheric pressure was specified, and the no-slip condition was posed on the model surface. In the structured calculation grid, the total number of calculation cells was about 800000. At the generatrix of the model, we had $Y^+ \le 2$.

In calculating the 3D flows around models in the T-500 wind tunnel, the calculation domain was a parallelepiped comprising part of the settling chamber, the nozzle, and the test section with the model and the diffuser. In the T-324 wind tunnel, the calculation domain was limited to the WT contour (Fig. 2). The boundary conditions specified in the calculations were described in the previous section. The total number of calculation cells in the unstructured grid was about 1400000.

Aerodynamic coefficients of the airfoil

The values of the aerodynamic coefficients $C_{x\mathrm{a}}$ and $C_{y\mathrm{a}}$ for the NASA0012 airfoil in T-500 and in T-324 at $\mathrm{Re_b} = 6.3\cdot10^5$, $0.2 \le \xi \le 0.6$, $\alpha = 5°$ and 10° are given in Table 1 ($\xi = b/l$).

The values of the relative increments of the aerodynamic coefficients of the airfoil $\Delta x = (C_{x\mathrm{a}}/C_{x\mathrm{af}} - 1)$ and $\Delta y = (C_{y\mathrm{a}}/C_{y\mathrm{af}} - 1)$ in T-500 and T-324 (here, the subscript "f" denotes

Table 1

WT	T-500				T-324			
b, m	0.1	0.15	0.2	0.3	0.2	0.25	0.3	0.4
ξ	0.2	0.3	0.4	0.6	0.20	0.25	0.30	0.40
$\alpha = 5°$								
$C_{x\mathrm{a}}$	0.012	0.015	0.018	0.023	0.0122	0.0129	0.0138	0.0155
$C_{y\mathrm{a}}$	0.432	0.396	0.361	0.302	0.431	0.423	0.414	0.396
$\alpha = 10°$								
$C_{x\mathrm{a}}$	0.018	0.0223	0.0263	0.0349	0.0182	0.0193	0.0206	0.0230
$C_{y\mathrm{a}}$	0.840	0.778	0.697	0.579	0.846	0.830	0.811	0.777
$C_{x\mathrm{o}}$	0.0084	0.0104	0.0122	0.0160	0.0084	0.0088	0.0094	0.0106

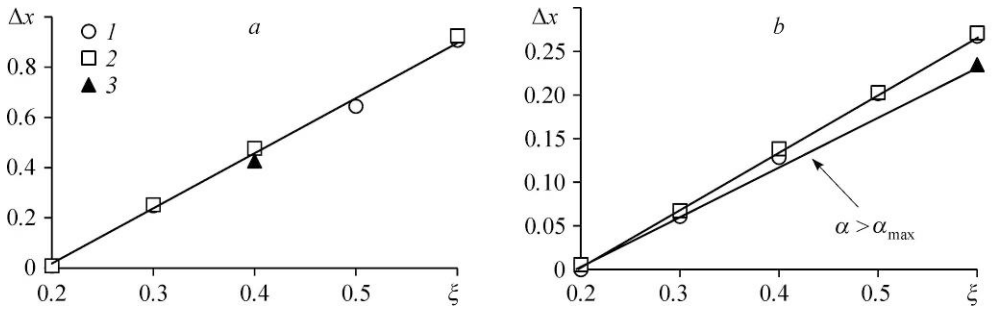

Fig. 3. Dependence $\Delta x\,(\xi)$ for the airfoil in T-500 (*a*) and T-324 (*b*) at $\mathrm{Re}_b = 6.3\cdot10^5$. $\alpha = 5°$ (*1*), 10° (*2*), and 20° (*3*).

the values of aerodynamic coefficients in the free stream) are shown in Figs. 3 and 4. The calculations have shown that for $\xi < 0.2$, the values of C_{xa} and C_{ya} in the free stream and in the WT test section are identical [13, 14]. The graphs prove that the dependences $C_{xa}(\xi)/C_{xaf}$ and $C_{ya}(\xi)/C_{yaf}$ can be fitted with a piecewise-linear function such that

$$F(\xi) = 1 \text{ for } 0 \le \xi \le \xi^* \text{ and } F(\xi) = 1 + A\,(\xi - \xi^*) \text{ for } \xi > \xi^*. \quad (1)$$

The dependence of the pitching moment ratio m_z/m_{zf} on ξ, not shown here, can also be fitted with a function of type (1). A comparison between the values of Δx and Δy at $\xi = \text{const}$ shows that the influence of the rigid walls of the closed test section on the values of C_{xa} and C_{ya} is notably smaller in comparison with the open test section.

Not only are the ratios of aerodynamic coefficients C_{xa}/C_{xaf} and C_{ya}/C_{yaf} linear in ξ, they are almost independent of the angle of attack, which fact is illustrated by the graphs in Fig. 5. The change of the values of $C_{xa}(\xi)/C_{xaf}$ and $C_{ya}(\xi)/C_{yaf}$ for $0 \le \alpha \le \alpha_{\max}$ is within 1.5 %, where the value $\alpha_{\max} = 15°$ refers to the maximum value of C_{ya} [13, 14]. The change of the regime of the flow around the airfoil at $\alpha > \alpha_{\max}$ leads to an insignificant decrease of the values of $\Delta x(\alpha)$ and $\Delta y\,(\alpha)$, which both remain close to a constant value.

The data on the increase of the lift force of the airfoil in the closed test section of AT-324 (see Fig. 4*b*) contradict the idea about the increased value of the lift force of the carrier model in the presence of rigid walls in comparison with the conditions of unbounded flow. For explanation of this contradiction, we performed the calculation of the flow around the airfoil using three calculation-domain configurations: the first configuration comprised a settling chamber, a nozzle, a 4-m long test section, and a diffuser; the second configuration, a settling chamber,

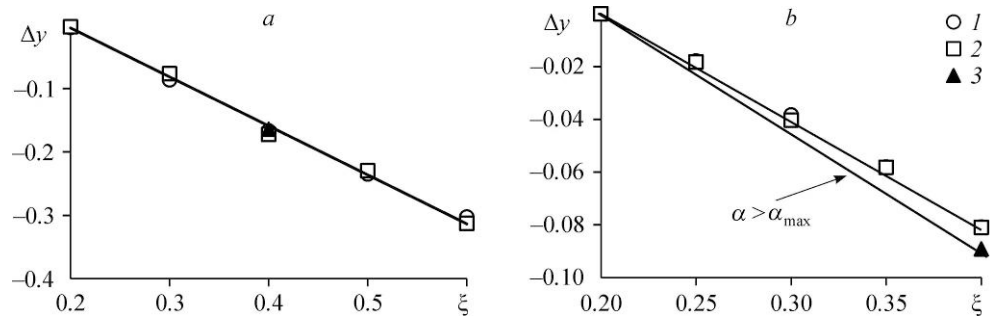

Fig. 4. Dependence $\Delta y\,(\xi)$ for the airfoil in T-500 (*a*) and T-324 (*b*) at $\mathrm{Re}_b = 6.3\cdot10^5$. $\alpha = 5°$ (*1*), 10° (*2*), and 20° (*3*).

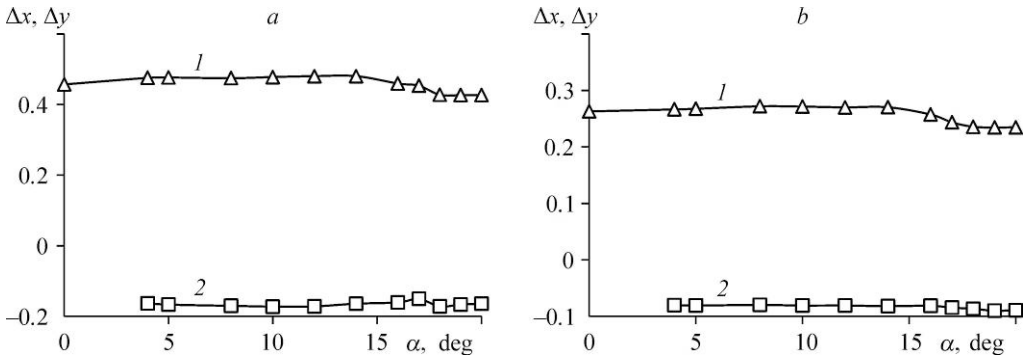

Fig. 5. Dependence of Δx and Δy on the angle of attack at $\xi = 0.4$ and $\mathrm{Re}_b = 6.3 \cdot 10^5$.
Open (*a*) and closed (*b*) test sections.

Table 2

Coefficients	Version 1	Version 2	Version 3	In free stream
C_{xa}	0.0230	0.0194	0.0206	0.0182
C_{ya}	0.777	1.05	1.086	0.846

a nozzle, a shorted test section of 2-m length, and a diffuser; and the third configuration, just a 4-m long test section, and no nozzle and diffuser. The values of the drag and lift coefficients of the airfoil at $\xi = 0.4$, $\mathrm{Re}_b = 6.3 \cdot 10^5$, and $\alpha = 10°$ are shown in Table 2, whose data illustrate the influence of the calculation domain on modeling results. In modeling the flow past the airfoil, in the short test section, in the presence of nozzle and diffuser (Version 2) as well as in the WT contour (Version 3), the rigid walls lead to an increase of the airfoil lift force in comparison with the conditions of an unbounded flow, which does not contradict both the experimental data and the classical theory [2, 8]. However, an increase of the test-section length (Version 1) leads to a reduction of airfoil lift force.

Drag coefficient of the cylinder

The performed calculations of the flow past a smooth circular cylinder immersed in a free stream have revealed a satisfactory agreement between calculated and experimental data. That agreement had proven it possible to use the SST model of turbulence in calculating the flows past circular cylinders [13].

The values of the drag coefficients of the cylinders of various diameters (D) in the test sections of the T-500 and T-324 wind tunnels at the number $\mathrm{Re}_D = 10^5$ are given in Table 3. The reduction of the values of C_{xa} observed on increasing the blockage factor ξ is related to the influence of the diffuser on the base pressure, which grows with increasing the diameter D.

The relative drag-coefficient increases $\Delta x\,(\xi)$ are shown in Fig. 6, whose graphs demonstrate the absence of the effect due to the boundaries of the open test section for $\xi = D/l \le \xi^* = 0.05$ and due to the boundaries of the closed test section for $\xi < \xi^* = 0.06$.

Table 3

WT	T-500				T-324			
D, mm	25	34	68	100	50	75	100	150
ξ	0.05	0.068	0.136	0.200	0.05	0.075	0.1	0.15
C_{xaf}	1.071	1.071	1.071	1.071	1.071	1.071	1.071	1.071
C_{xa}	1.069	1.010	0.840	0.702	1.070	1.046	1.012	0.935

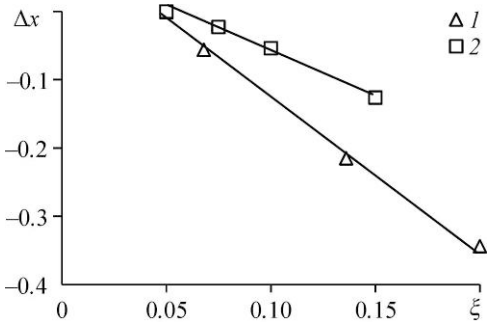

Fig. 6. Increases of the drag coefficient of cylinder $\Delta x(\xi)$ at $\mathrm{Re}_D = 10^5$. Open (*1*) and closed (*2*) test section.

For $\xi > \xi^*$, the incremental changes Δx vary in proportion to ξ, and the ratio $C_{xa}(\xi)/C_{xaf}$ can be fitted with a linear dependence of form (1). Like in the case of the airfoil, the effect due to the rigid walls of the closed test section on the values of C_{xa} is much less pronounced in comparison with the open test section.

Influence of the size of the model on the values of its aerodynamic coefficients in 3D flows

Consider three models possessing a high value of drag resistance (Fig. 7). A common feature of the flows around these models is the formation of a developed base-wake separation due to the stall of the stream from the edges of the front shield (models of Figs. 7*a* and 7*b*, where *R* is the radius of the sphere) and the stern cone (model of Fig. 7*c*). The first two models are shaped as segmented cones with different vertex angles of the stern cone and different front-shield radii. In calculation of aerodynamic coefficients, as the characteristic length, we used the diameter of the front shield or that of the stern cone; as the characteristic area, the drag area $S_\mathrm{d} = \pi D^2/4$; and as the momentum point, the leading stagnation point on the model at $\alpha = 0$. The angle of attack was set by rotating the model around its central point.

A comparison between the experimental and calculated values of the aerodynamic coefficients for the model of Fig. 7*c* [17] (see Fig. 8) and that for the model of Fig. 7*a* (see [9]), demonstrates their satisfactory agreement and points to the adequacy of the mathematical model adopted for the flow. Note that the experimental data refer to the case of $\xi = 0.026$. The influence of the size of the model of Fig. 7*a* on the values of its aerodynamic coefficients in T-500

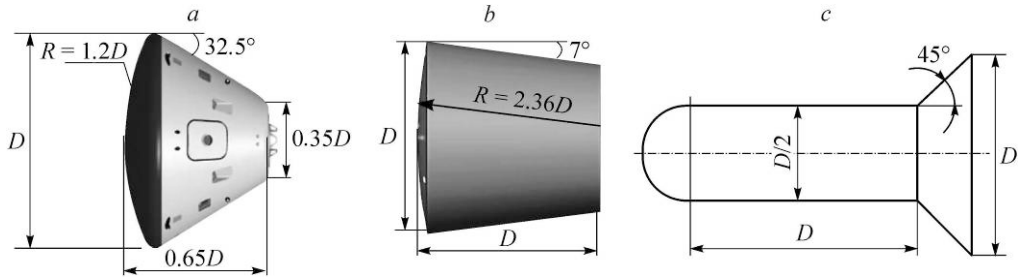

Fig. 7. Shapes of examined models.

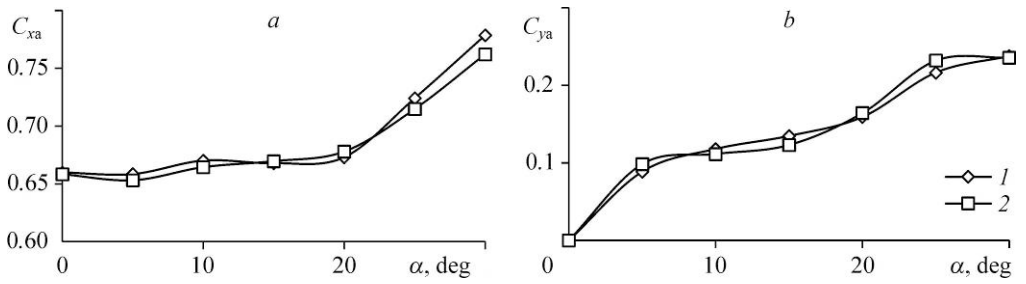

Fig. 8. Dependences of C_{xa} and C_{ya} on the angle of attack for the model of Fig. 7*c* at $\mathrm{Re}_D = 3 \cdot 10^5$.

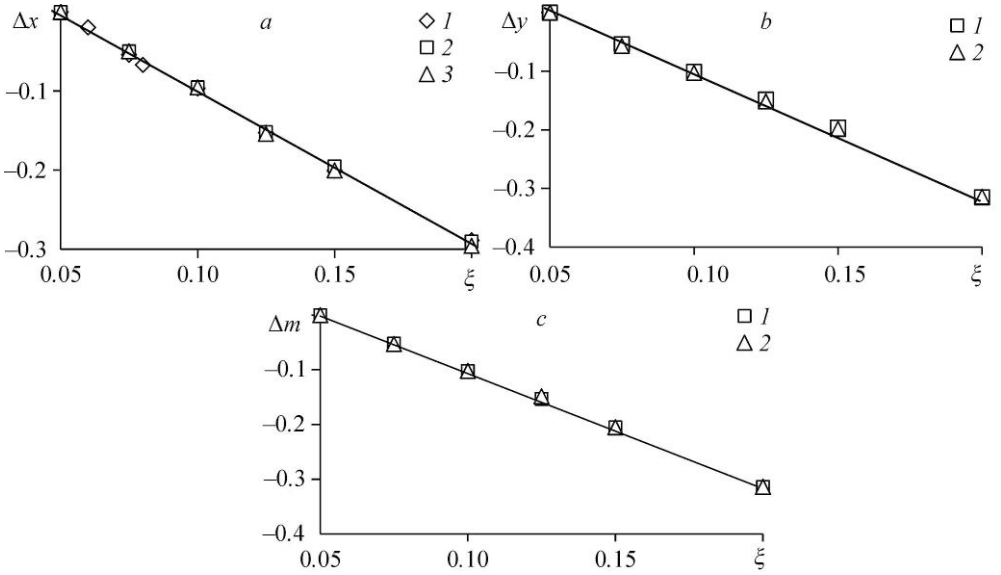

Fig. 9. Dependences of Δx, Δy, and Δm on ξ for the model of Fig. 7*a* in T-500. $\mathrm{Re}_D = 4 \cdot 10^5$; *a* — $\alpha = 0°$ (*1*), 10° (*2*), and 20° (*3*), *b*, *c* — $\alpha = 10°$ (*1*) and 20° (*2*).

is illustrated in Fig. 9 with graphs that show the dependences of Δx, Δy, and Δm on the blockage factor ξ. Also reflected in the graphs is the linear dependence of the aerodynamic coefficients on the blockage factors ξ for $\xi > 0.05$ (in the case of $\xi < 0.05$, the aerodynamic coefficients of the model are independent of its size). In the analyzed range of the angles of attack, the effect of this angle on the ratios $C_{xa}(\xi)/C_{xaf}$, $C_{ya}(\xi)/C_{yaf}$, and $m_z(\xi)/m_{zf}$ is insignificant (see Fig. 10).

Linear behaviors are also exhibited by the dependences $\Delta x(\xi)$, $\Delta y(\xi)$, and $\Delta m(\xi)$ for the models shown in Figs. 7*b* and 7*c*. For all the three models, the values of Δx, Δy, and Δm at $\xi = \text{const}$ are roughly identical, which fact is evident from Table 4, which shows the data calculated for $\xi = 0.2$ and $\alpha = 20^o$. The graphs of Fig. 9 and the data of Table 4 show that, in the open test section, the ratios $C_{xa}(\xi)/C_{xaf}$, $C_{ya}(\xi)/C_{yaf}$, and $m_z(\xi)/m_{zf}$ show a decrease on increasing the model size. It can easily be seen that, due to the linearity of the dependences $\Delta x(\xi)$, $\Delta y(\xi)$, and $\Delta m(\xi)$, identical or close values of these quantities at $\xi = \text{const}$ imply the independence of the position of the pressure center of the model of the model size in the open test section, at least for $\xi \le 0.2$. In the closed test section, the increments Δx, Δy, and

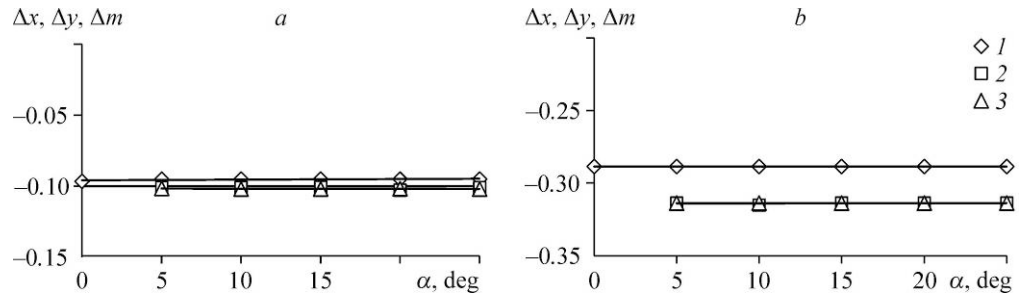

Fig. 10. Changes Δx, Δy, and Δm for the model of Fig. 7*a* versus the angle of attack at $\xi = \text{const}$. $\xi = 0.1$ (*a*) and 0.2 (*b*); *1* — Δx, *2* — Δy, *3* — Δm.

Table 4

Values of Δx, Δy, and Δm of the models at $\xi = 0.2$ and $\alpha = 20°$

WT	T-500			T-324		
Model	7*a*	7*b*	7*c*	7*a*	7*b*	7*c*
Δx	–0.272	–0.282	–0.296	0.462	0.433	0.421
Δy	–0.272	–0.281	–0.314	0.371	0.380	0.341
Δm	–0.272	–0.283	–0.314	0.132	0.121	0.124

Δm are positive [9], leading to the growth of the ratios of $C_{xa}(\xi)/C_{xaf}$, $C_{ya}(\xi)/C_{yaf}$, $m_z(\xi)/m_{zf}$ for the analyzed models with increasing the value of ξ.

Experimental results

Dependences of form (1) also arise in the physical modeling in wind tunnels. Results of the treatment of data gained in WT studies aimed at the determination of the drag coefficients of parachute models of various permeabilities (7, 15, and 30 %) in six subsonic wind tunnels [6] are shown in Fig. 11, where the bracketed figures indicate the accuracies in the determination of the coefficient C_{xa}. Evidently, the experimental data can be fairly well fitted with the piecewise-linear dependence (1). For parachute permeabilities of 7, 15, and 30 %, we have, respectively, $\xi^* = 0.072$, 0.066, and 0.054.

An analysis of data gained in WT tests of a model rectangular wing of aspect ratio $\lambda = 6$ and a flap reclinated by an angle of 60° at $\xi = 0.16$ and $\xi = 0.016$ [18] shows that the ratios $C_{xa}(\alpha)/C_{xaf}$, $C_{ya}(\alpha)/C_{yaf}$, and $m_z(\alpha)/m_{zf}$ weakly depend on the angle of attack, this result being illustrated with graphs of Fig. 12. In the latter case, the blockage factor ξ is defined as the ratio between the wing area and the cross-sectional area of the test section. Note that the coefficient C_{yamax} corresponds to the angle $\alpha = 8°$ at $\xi = 0.16$ and to the angle $\alpha = 11.5°$ at $\xi = 0.016$. The deviation of $C_{xa}(\alpha)/C_{xaf}$ from the average value of this ratio is within 2 %, whereas the values $C_{ya}(\alpha)/C_{yaf}$ and $m_z(\alpha)/m_{zf}$ are almost constant and do not depend on the angle α.

Conclusion

The performed study has allowed us to establish the functional dependence of the aerodynamic coefficients of a model on the factor of blockage of the WT test section with this model in low-speed subsonic wind tunnels. The ratios of the aerodynamic coefficients of the model in the WT test section and in the free stream can be approximated with a piecewise-linear function of the blockage factor equal to unity at low values of this factor. The values of this function are almost independent of the angle of attack in the examined range

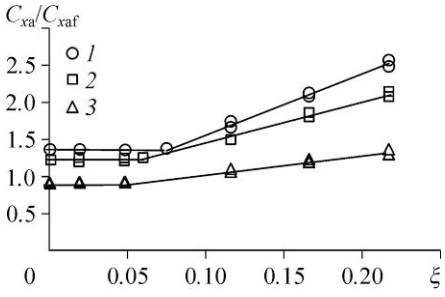

Fig. 11. The drag coefficient of parachute models of various permeability [6].

Permeability 7 % (Δ = ± 0.04) (*1*), 15 % (Δ = ± 0.03) (*2*), 30 % (Δ = ± 0.03) (*3*).

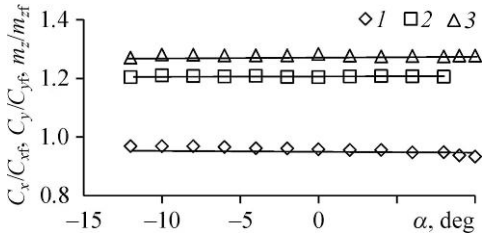

Fig. 12. Dependence of $C_{xa}(\alpha)/C_{xaf}$, $C_{ya}(\alpha)/C_{yaf}$, and $m_z(\alpha)/m_{zf}$ ratios on the angle of attack according to the experimental data of [18].

1 — C_x/C_{xf}, *2* — C_y/C_{yf}, *3* — m_z/m_{zf}.

of angles, and they can be either higher or lower than unity depending on the WT test-section type and its length. The lift force of the airfoil in the closed test section depends on the test section, whose increase reduces the lift force of the airfoil in comparison with free-stream conditions.

References

1. **A.N. Evgrafov and A.V. Kutyaev,** A method for taking into account the effect of wind-tunnel test section cluttering on the aerodynamic drag of car, Izv. MGIU, ser. Mashinostroenie, 2006, No. 1, P. 70–73.
2. **S.M. Gorlin and I.I. Slezinger,** Aerodynamic Measurements: Methods and Instrumentation, Nauka, Moscow, 1964.
3. **W.H. Rae, Jr. and A. Pope,** Low-Speed Wind Tunnel Testing, John Wiley and Sons, 2nd ed., 1984.
4. **E.C. Maskell,** A theory of the blockage effects on bluff bodies and stalled wings in a closed wind tunnel, ARC R and M, 1965, No. 3400.
5. **B.N. Yuriev,** Experimental Aerodynamics, Pt. 2, Oborongiz, Moscow 1939.
6. **A.N. Evgrafov,** Method for carrying-over the results of model tests to a full-scale car, Izv. MGIU, ser. Mashinostroenie, 2007, No. 2, P. 21–24.
7. **J.M. Macha and R.J. Buffington,** An experimental investigation of wall-interference effects for parachutes in closed wind tunnels, Sandia Report SAND89-1485, Sandia National Laboratories, Albuquerque, NM, USA, Dec. 1985.
8. **B.F.R. Ewald,** Wind tunnel wall corrections, AGARDograph, 1998, No. 336.
9. **B.T. Bui, V.T. Kalugin, and A.I. Khlupnov,** Correction of weighing-test results of a model as applied to the free-flow conditions at low subsonic velocities, Kosmonavtika i Raketostroenie, 2016, No. 1, P. 86–93.
10. **A.G. Golubev, V.T. Kalugin, A.Yu. Lutsenko, A.I. Khlupnov et al.,** Aerodynamics, V.T. Kalugin, (Ed.) Bauman Moscow State Techn. Univ., Moscow, 2010.
11. **N.F. Polyakov,** A method for studying the flow characteristics in a low-turbulence wind tunnel and the transition phenomena in incompressible boundary layer. Diss. Cand. Tech. Sci., Novosibirsk, 1973.
12. **V.T. Bui,** Analysis of the flow around an airfoil in the test section of a low-velocity wind tunnel, Vestnik MGTU, ser. Mashinostroenie, 2013, No. 4, P. 109–119.
13. **V.T. Bui and V.N. Lapygin,** Simulation of the flow past a model in the closed test section of a low-velocity wind tunnel and in the free stream, Thermophysics and Aeromechanics, 2015, Vol. 22, No. 3, P. 351–358.
14. **V.T. Bui and V.N. Lapygin,** Model size influence on its aerodynamic coefficients in low speed wind tunnel, Mathematical Models and Computer Simulations, 2015, Vol. 7, No. 6, P. 593–600.
15. **A.M. Kharitonov,** Techniques and Methods of Aerophysical Experiment, Pt. 1, Wind Tunnels and Gas-Dynamic Facilities, Novosibirsk State Technical University Publ., Novosibirsk, 2005.
16. **I.A. Belov and S.A. Isaev,** Modeling of Turbulent Flows: A study guide, St.-Petersburg, Baltic University Publ., 2001.
17. **V.Yu. Sobolev,** A procedure for determining the aerodynamic characteristics of aircrafts with stabilizing devices in a subsonic flow with separation, Diss. Cand. Tech. Sci.: defended 06.08.2007: approved 10.26.2007, Moscow, 2007.